J. Fluid Mech. (1980), *vol.* 101, *part* 2, *pp.* 243–256
Printed in Great Britain

The instantaneous velocity fields of coherent structures in coflowing jets and wakes

By A. E. PERRY, T. T. LIM AND M. S. CHONG

Department of Mechanical Engineering, University of Melbourne, Parkville, Victoria, Australia

(Received 30 April 1979 and in revised form 31 March 1980)

The instantaneous velocity vector fields which surround the coherent structures of Perry & Lim (1978) in coflowing jets and wakes have been successfully measured and related to the smoke patterns for Reynolds numbers of order 1000. By the use of critical point theory, a qualitative description of the three-dimensional flow field can be made and is applied to the simplest structures which were classified by Perry & Lim. From these results, the convection of smoke and vorticity from the source and the entrainment properties of the structures are discussed.

1. Introduction

Recently Perry & Lim (1978) studied forced periodic coflowing jets and wakes at Reynolds numbers of the order 1000. By laterally perturbing sinusoidally a glass tube from which smoke was issuing into an outer coflowing external stream, they found that the naturally occurring random eddying motions could be locked in with the perturbing frequency. When viewed under stroboscopic light of the correct frequency, the eddy structures appeared frozen in time. The geometry of the three-dimensional smoke patterns could be examined in great detail using strobed laser beams. From this work a classification of the simplest occurring structures was made and an updated version is shown in figure 1. The structures can be double sided or single sided. The single-sided ones are the result of either buoyancy effects or how the vorticity has been generated at the source. In the case of wakes the eddies point downstream and in the case of jets the eddies point upstream. It was conjectured that these patterns might be similar to the large-scale structures of fully turbulent jets and wakes. The results of Cantwell (1975) on the turbulent near wake of a circular cylinder at a Reynolds number of 140000 suggest this to be true. Recent work carried out at Melbourne by Perry & Watmuff (1981) on the wakes behind three-dimensional bodies at high Reynolds numbers also confirmed this sugestion. The fine-scale motions which are superimposed on the large-scale motions are apparently 'decoupled' to some extent and the broad features of the large-scale motions are not greatly altered.

The work of Perry & Lim was confined to an examination of the smoke patterns. These patterns give an idea of the vorticity distribution since the outer edge of the smoke is a vortex sheet (at least before viscous diffusion becomes significant). It has been the aim of many people to measure an entire instantaneous velocity vector field surrounding eddying motions and to relate this field with the smoke patterns (e.g. see Davies & Yule 1975 and Falco 1977). The fact that the eddy structures of Perry & Lim

0022-1120/80/4595-2510 $02.00

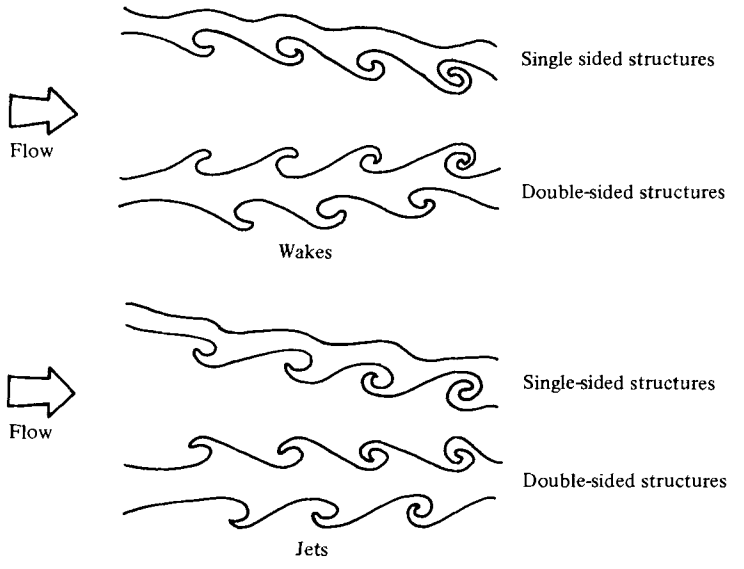

FIGURE 1. Classification of simple coflowing wake and jet structures. Flow issuing from tube. Only sections contained in centre-plane are shown.

can be made perfectly periodic in time affords a unique opportunity to make such measurements in great detail using a conditional sampling technique based on the phase of the disturbing oscillation. By means of an on-line digital computer, an entire vector flow field on the plane of symmetry of the structures can be obtained from hot-wire measurements in a time of approximately seven minutes.

One of the problems with velocity fields is that the geometry depends on the velocity of the observer and it would be better to use an invariant quantity. Vorticity is such a quantity but is extremely difficult to measure. Cantwell (1978) and Cantwell, Coles & Dimotakis (1978) applied similarity transformations to measured flow fields to obtain invariant patterns. In any case, even a qualitative knowledge of the instantaneous vector flow fields, as seen by an observer moving with the structures, gives an insight into the entrainment processes and the large-scale transport processes.

Three-dimensional flow fields are extremely complex and are most difficult to describe in detail. However, there are certain features of flow fields known as 'critical points' which form the salient features of these patterns. Once these critical points are located and identified, all the essential features of the flow geometry can be deduced. Critical-point theory (also known as the 'phase-plane' or 'phase-space' method) was applied by Oswatitsch (1958), Davey (1961) and Lighthill (1963) to viscous flow close to a rigid boundary. Smith (1972) applied this theory to conical flows. Perry & Fairlie (1974, 1975) extended the approach to inviscid rotational flow close to and away from boundaries. Hunt *et al.* (1978) extended the work of Perry & Fairlie and made studies of flow around obstacles attached to surfaces. Cantwell *et al.* (1978) applied the critical-point theory to the geometry of turbulent spots.

The flow field surrounding the structures studied by Perry & Lim (1978) are reported here and are described with the aid of critical-point theory.

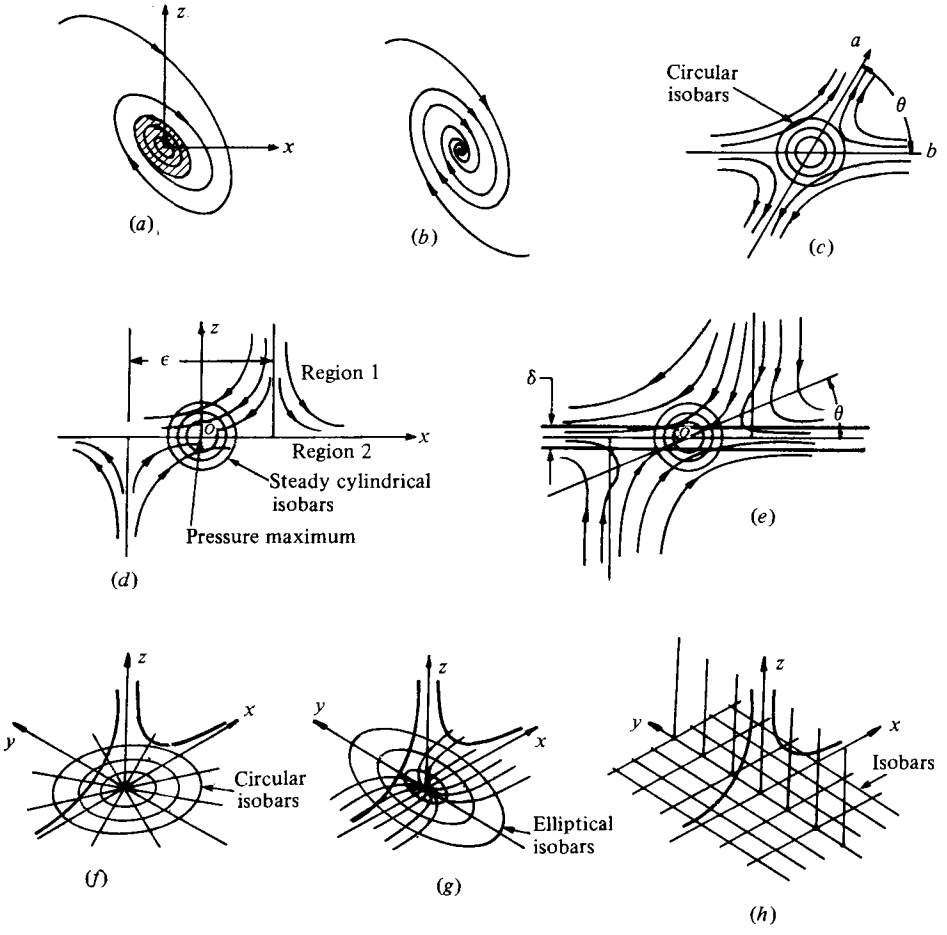

FIGURE 2. (*a*) Constant vorticity inviscid centre; (*b*) focus; (*c*) constant vorticity saddle *a* and *b* are eigenvectors; (*d*) dislocated saddle; (*e*) dislocated saddle with a finite-thickness sheet of thickness δ; (*f*) axisymmetric stagnation point; (*g*) general three-dimensional stagnation point; (*h*) two-dimensional stagnation point. Isobars are shown in the x, y plane for (*f*), (*g*) and (*h*).

2. Critical-point theory

A critical point is a point in a flow field in which the trajectory slope (or instantaneous streamline slope) is indeterminate. The patterns and their properties are obtained from the spacewise linearized solution of the Navier–Stokes and continuity equations. For the work here, the inviscid critical points of Perry & Fairlie (1974) need to be extended.

In figure 2 (*a*) is shown a centre (shaded region). In three dimensions the trajectories can 'in the large' spiral in but must asymptote to closed trajectories as the centre is approached. The vorticity vector is orthogonal to the plane containing the trajectories and the flow is locally two-dimensional close to the centre. A centre corresponds with a pressure minimum. It is assumed that the vorticity is constant in space and time close to the centre and therefore vortex stretching is small.

If vortex stretching is included the pattern becomes unsteady and we have a focus

as shown in figure 2(*b*). For all cases considered here, the effect of vortex stretching is small.

Figure 2(*c*) shows a constant vorticity saddle and it can be seen that the eigenvectors labelled *a* and *b* are non-orthogonal. Again the flow is locally two-dimensional and, if the flow is steady, saddles correspond to pressure maxima. For all cases considered so far the second derivatives of kinematic pressure $P_{xx} = P_{zz}$ and the isobars are concentric cylinders and pressure varies parabolically with radius. The angle θ of the eigenvectors shown in figure 2(*c*) is given by $\tan\theta = 2\sqrt{(-P_{xx})}/\eta$, where η is the vorticity.

In figure 2(*d*) we have a new type of critical point which will be referred to as a dislocated saddle. Such a critical point sits on a vortex sheet and the 'dislocation' is possible because of the discontinuity at the sheet. Irrotational saddles sit on either side of the sheet. The flow pattern is unsteady since the sheet of spacially uniform strength is being stretched in a direction across the filaments and the sheet strength diminishes with time. The velocity field on either side of the sheet is given by

$$u = ax \mp \tfrac{1}{2}a\epsilon_0 e^{-at}, \quad w = -az, \tag{1}$$

where u and w are the x and z velocity components and a is invariant with time and is given by $a = \sqrt{-P_{xx}} = \sqrt{-P_{zz}}$. The minus and plus sign in equation (1) corresponds with regions (1) and (2) shown in figure 2(*d*) respectively. Again the isobars are concentric cylinders about the origin O and correspond with a pressure maximum. Also ϵ_0 is the dislocation distance ϵ in figure 2(*d*) when $t = 0$. Equation (1) represents a piecewise linearized solution of the Navier–Stokes equation and is consistent with the conservation of angular momentum of particles within the sheet. As the sheet is stretched, the two saddles approach each other exponentially and this irregular critical point ultimately becomes a regular irrotational saddle with orthogonal eigenvectors. If a finite thickness sheet is assumed, then, close to O, a regular constant vorticity critical point is formed as shown in figure 2(*e*) which is the same as in figure 2(*c*). This, in the large, would merge into the pattern shown in figure 2(*d*).

Some further critical points which are needed and which were not discussed by Perry & Fairlie (1974) are the three-dimensional irrotational node–saddle combinations shown in figures 2(*f*), (*g*) and (*h*). By redoing the analysis of Perry & Fairlie for irrotational flow, these solutions occur. All eigenvector planes are orthogonal and in figure 2(*f*) we have an axisymmetric stagnation point with a star node in the x, y plane. Figure 2(*g*) shows a general node in the x, y plane and figure 2(*h*) is the two-dimensional stagnation point flow. The shape of the node is determined by external far-field boundary conditions. The isobars in general are ellipsoids but are cylindrical in figure 2(*h*).

3. Experimental procedure and results

Velocity fields of coflowing wakes have been measured using crossed hot wires and conditionally sampling the data on the basis of phase. Figure 3 shows the method of data sampling. A vertical traverse of the structures was made at their plane of symmetry. A picture could be produced of the instantaneous vector field at a given phase by assuming that horizontal distances are time like. By traversing at two stations one wavelength apart, ratios of length and velocity scales can be found from the temporal mean profiles. Also the spreading angles of the structures could be measured from

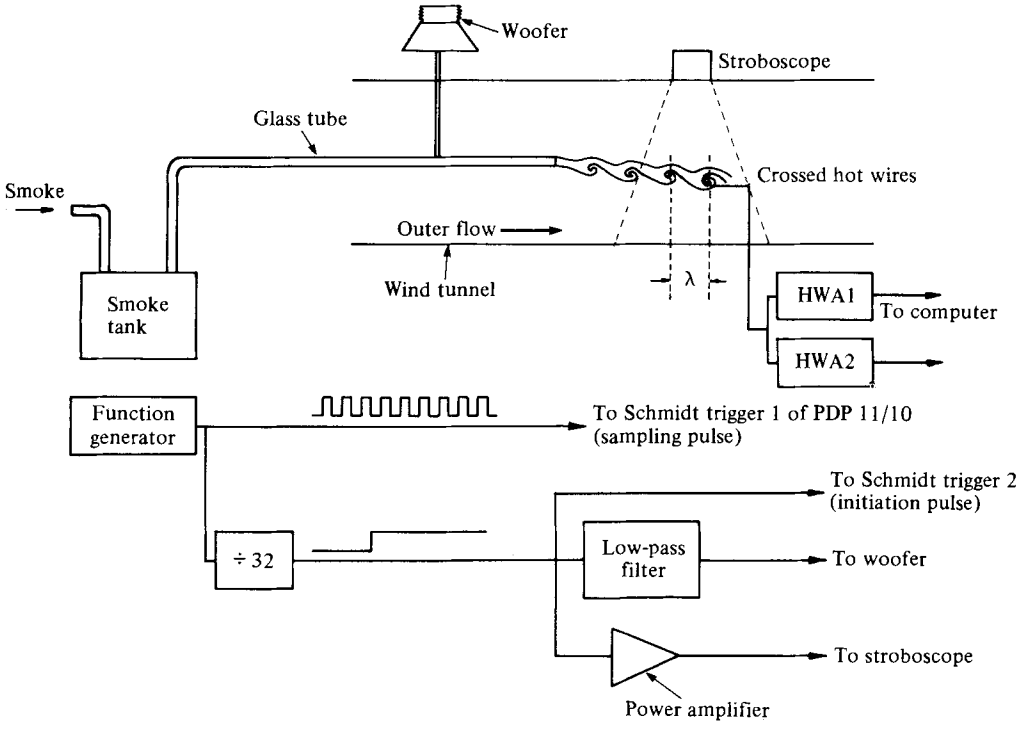

FIGURE 3. System used for data sampling coflowing jets and wakes. HWA means hot-wire anemometer.

photographs. This information can be used so that the plots can be distorted by linear weighting factors which give plots which correspond to the geometry of the smoke pictures. Details of the hot-wire anemometry and data reduction are given in Lim (1979). Signals from the wires were scaled by a dynamic matching procedure. Since the tunnel velocities were very low (typically 0·5 to 2 m s^{-1}) it was necessary to use the vortex-shedding method of Roshko (1954) for the purpose of measuring the tunnel velocity during the static calibration of the hot wires.

Figure 4 (plate 1) shows a single-sided coflowing wake (negatively buoyant wake) together with the phased-averaged vector field. Because these structures are so periodic in time, only ten data points were averaged for each point in the flow field. The structures remained steady only for a limited time (about seven minutes). They tended to drift as the smoke tank emptied. It was therefore difficult to register the patterns precisely with the smoke and a more rapid data sampling method is needed. The phase velocity U_ϕ of the observer was calculated from $U_\phi = f\lambda$, where f is the frequency of shaking and λ is the wavelength of the structures. A small vertical downward phase velocity was introduced,

$$U_{\phi_v} = U_\phi s/\lambda,$$

where s is the vertical distance the measured mean velocity defect peak shifted downward over one wavelength λ of the structures. Although these structures grow and develop with streamwise distance, it was found that the wavelength λ was essentially constant.

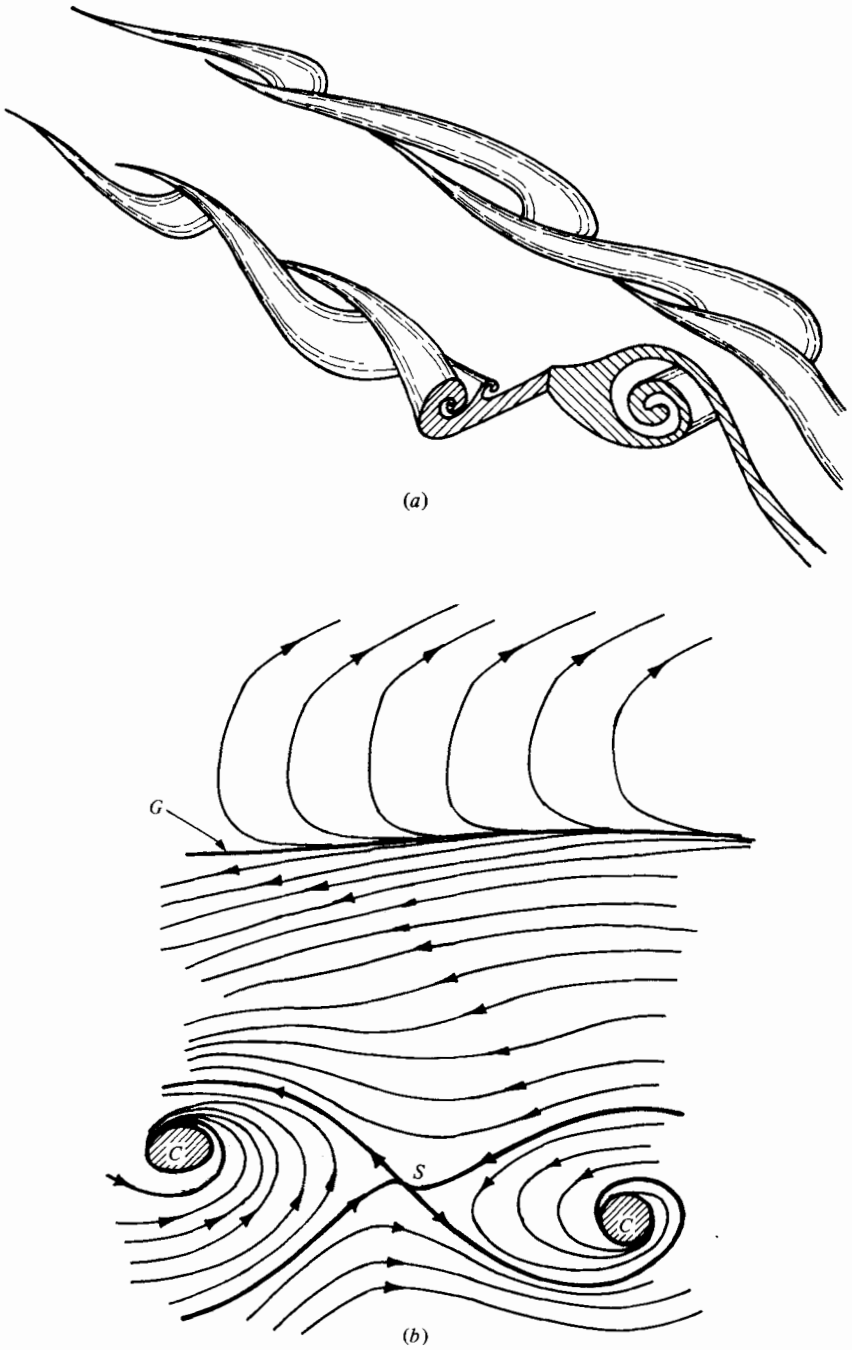

FIGURE 5. (*a*) Geometry of negatively buoyant wake structure as deduced from Perry & Lim (1978). (*b*) Streamline pattern deduced from figure 4 (*b*). Separatrices are shown in as heavy lines. *S*, saddles; *C*, centres; *G*, singular trajectory.

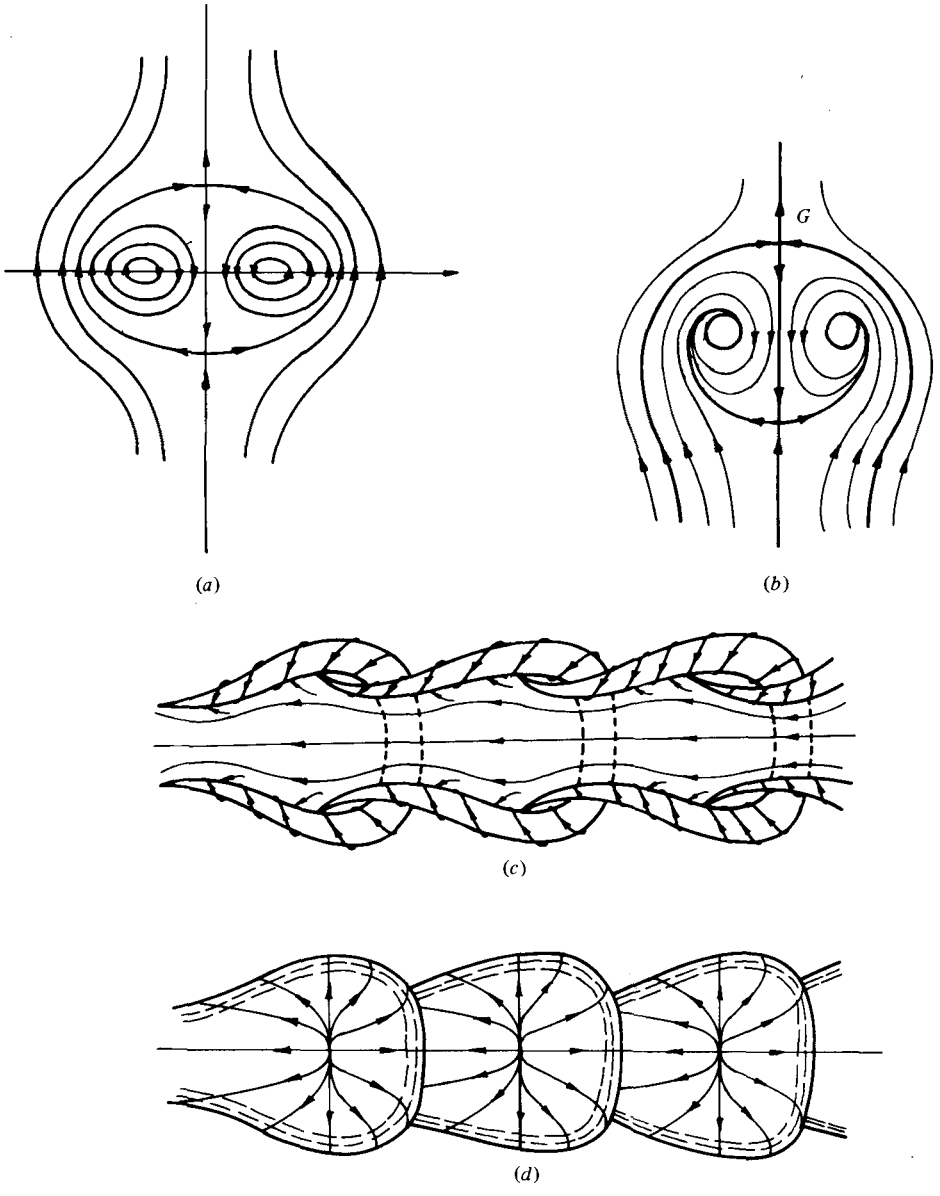

FIGURE 6. (*a*) Two-dimensional flow field generated by a vortex pair relative to an observer moving with the pair. (*b*) conjectured pattern of projections of vectors on cross-flow plane of structures given in figure 5. (*c*), (*d*) conjectured patterns on or near the surface of the smoke. (*c*) view from above, (*d*) view from below. Vortex sheet assumed to have zero thickness (see text).

Figure 5(*a*) shows the geometry of the structures as deduced from Perry & Lim (1978). The initially cylindrical vortex tube is folded and deformed without any holes or bifurcations. Assuming that the structures when viewed by an observer moving at the correct convection velocity are quasi-steady the critical points discussed in § 2 can be identified. Centres and dislocated saddles are apparent although viscous diffusion and slight phase jitter has caused these saddles to have the 'smeared out' appearance

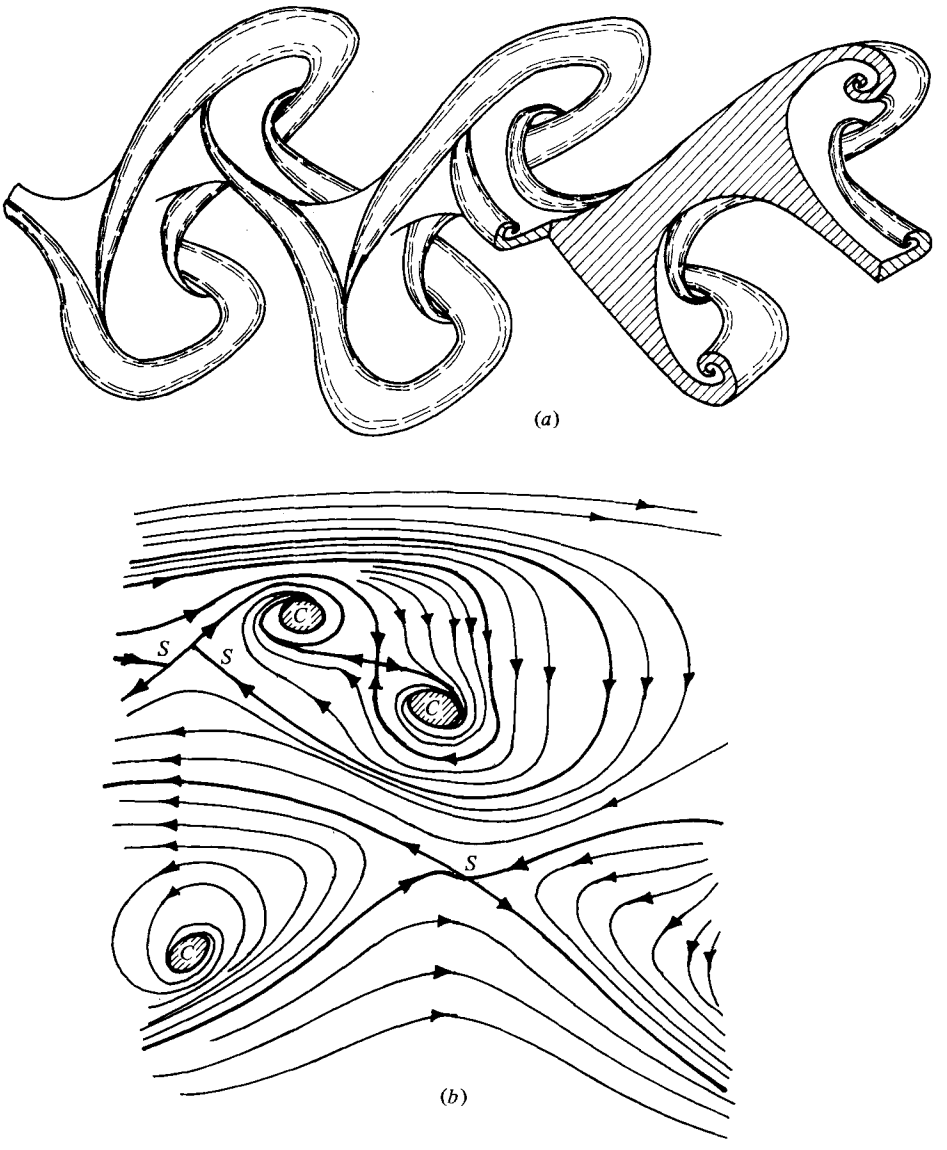

FIGURE 8. (*a*) Smoke geometry of a simple neutrally buoyant wake structure (no split eddies) as deduced from Perry & Lim (1978). (*b*) Streamline pattern deduced from figure 7 (*b*). Separatrices are shown in as heavy lines.

shown in figure 2(*e*). The separatrices (trajectories which emanate from saddles) are shown heavy and divide the pattern up into zones.

Above these structures there exists a singular trajectory labelled G which forms an asymptote for neighbouring trajectories. This singular trajectory is the intersection of a stream surface with the plane of symmetry and by continuity one can deduce what the projected flow pattern looks like in the end view. These structures have a pattern in the end view similar to that of two trailing vortices. If the observer

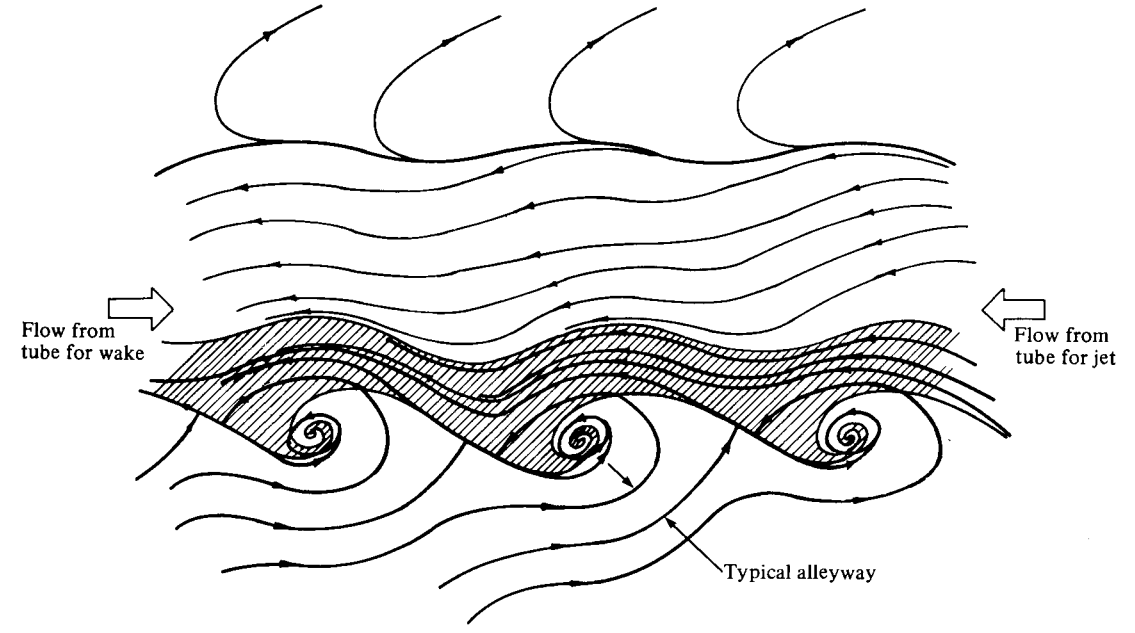

(*a*)

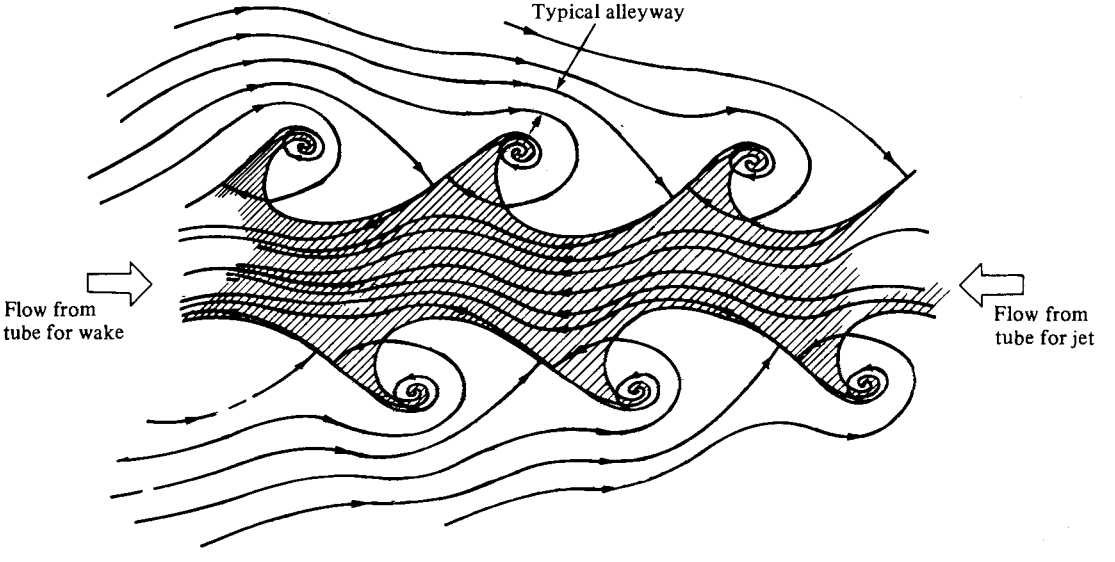

(*b*)

FIGURE 9. (*a*) Negatively buoyant wake for flow from left to right. For positively buoyant wake, simply reflect figure about a horizontal axis. If streamwise growth rate is ignored, figure also corresponds to negatively buoyant jet for flow from tube from right to left. For positively buoyant jet, again reflect figure about a horizontal axis. (*b*) Neutrally buoyant wake for flow from left to right. For neutrally buoyant jet, flow is from right to left. For both (*a*) and (*b*), the observer is moving with the structures. Streamwise development of these structures is not shown.

moves with these vortices as they convect themselves downwards, the pattern shown in figure 6(*a*) would be produced. The separatrix surrounding the vortex pair is closed. However, the structures possess three-dimensionality and hence there is a net divergence of the vector field in this end plane and the separatrix is open as shown in figure 6(*b*). Fluid is entrained into these structures from below the singular streamline labelled *G* (see also figure 5). Figures 6(*c*) and (*d*) show the conjectured streamline patterns on or near the surface of the smoke.

The analysis which leads to equation (1) is only for two-dimensional flow. Strictly speaking, the dislocated saddle in figure 5(*b*) is three-dimensional. Assuming viscous diffusion were absent, a zero-thickness vortex sheet would result and we would have associated with it a general node of the type given in figure 2(*g*) on either side of the sheet. One set of such nodes is shown in figure 6(*d*). A corresponding set is on the inside surface of the tubular sheet and is hidden from view. If the vortex sheet is of finite thickness, the dislocated saddle, in the small, becomes a regular constant vorticity saddle of the type shown in figure 2(*c*) and (*e*). The flow then becomes locally two-dimensional and a degenerate node of the type given in figure 2(*h*) would result and would be in a plane inside the sheet.

Figure 7 (plate 2) shows the smoke pattern and associated vector field of a double-sided wake. Unfortunately, the only pattern of this kind which could be produced for a sufficient time for the data sampling possessed a split or double eddy at the top. Figure 8(*a*) shows the ideal smoke pattern as deduced from Perry & Lim (1978) while figure 8(*b*) shows the actual streamline pattern deduced from figure 7(*b*). An outer singular trajectory corresponding with *G* in figure 5 is absent since the observer is moving horizontally.

We have now sufficient information to deduce the patterns for all flow cases classified by Perry & Lim (1978) including the jets. These are summarized schematically in figure 9 with the conjectured smoke pattern superimposed (shown shaded).

Figure 10(*a*) (plate 3) shows flow over a rivet head (a dome-shaped body attached to a boundary). It can be seen from the dye that a single-sided wake structure is produced similar to the one shown in figures 5 and 9(*a*) except it is inverted. The orientation of the loops is due entirely to the sign of the vorticity generated at the source and not the result of buoyancy. Figure 10(*b*) shows streaklines and a dislocated saddle is evident although streaklines should be interpreted with caution. Like Hunt *et al.* (1978), the authors found that details in the cavity were Reynolds number dependent.

4. Discussion of results

4.1. *Transport of smoke*

From figure 9 it can be seen that instantaneous streamlines can cross vortex sheets and must do so with a discontinuity at the sheet. The initial cylindrical vortex sheet is unsteady and can move normal to itself. The smoke which is bounded by this sheet is being squeezed backwards relative to the moving observer (in the case of a wake) in much the same way as toothpaste would be squeezed along in a very flexible tube until finally the tube is squeezed to a very small thickness. All that is finally left after a sufficient development is the outer shell where most of the vorticity resides. A great

deal of vortex stretching and vorticity cancellation by viscous diffusion must occur during this process. The separatrices form instantaneous alleyways of fluid which penetrate through the vortex sheet and back up along the smoke.

The dislocated saddles, which have been smeared by viscous diffusion, are features which also appear in the calculated two-dimensional patterns of Corcos & Sherman (1976) for the roll-up of an initially plane vortex sheet. The use of constant vorticity centres to represent the pattern assumes that vorticity has diffused in the region of the roll-up, giving a uniform blob of vorticity.

Perry & Lim (1978) found that the smoke patterns of coflowing wakes are similar to those behind a sphere and so the vector field results should be applicable to spheres (see also Achenbach 1974 and Taneda 1978). The deformed 'smoke tube' would consist of boundary-layer material from the sphere.

4.2. *Entrainment and mixing*

Cantwell *et al.* (1978) discussed the difficulties with the definition of entrainment and mention some alternatives to the conventional definition. The present authors are going to use the conventional definition according to Head (1960) and Head & Bradshaw (1971), i.e. entrainment is the volume rate of fluid which is infected with mean vorticity. In figure 9 fluid which spirals in towards centres or moves down alleyways is often said to be entrained. However, entrainment is possible without this process occurring. A simple example of this is the ideal spacially periodic two-dimensional Kelvin/Helmholtz-like roll-up of a shear layer. Figures 11(*a*), (*b*) and (*c*) shows its conjectured progress as it rolls up with separatrices shown. Since the flow is two-dimensional foci are not possible by continuity. This is the pattern as seen by an observer moving with the eddies. It is growing with time but not with x. There are then various ways of defining mean flow and mean vorticity. Here, the mean flow will be defined as the spacial average in the x direction and would correspond with a short time average for an observer moving very rapidly relative to the structures in the x direction. All mean streamlines are then straight and horizontal. Although the shear layer possesses a displacement thickness which is growing with time, the streamlines are not displaced, i.e. the vertical component of mean velocity is zero since by continuity

$$\frac{v}{U_1} = \frac{d\delta^*}{dx} = 0,$$

where δ^* is the displacement thickness defined as

$$\delta^* = \int_0^\infty \left(1 - \frac{U}{U_1}\right) dz.$$

It can be seen that, as the sheet rolls up, the separatrices propagate out through the fluid like a wave. The boundaries (shown as A in figure 11*c*) define the region where the mean streamlines possess mean vorticity and these boundaries are propagating outwards at some velocity q. Hence the entrainment, i.e. the volume of fluid per unit streamwise and spanwise length crossing the boundaries, is $2q$. This will be referred to as entrainment of the first kind.

The regions shown shaded in figure 11(*b*) are mixing zones. These are defined as those regions where trajectories are closed. Any fluid interface in this region will be

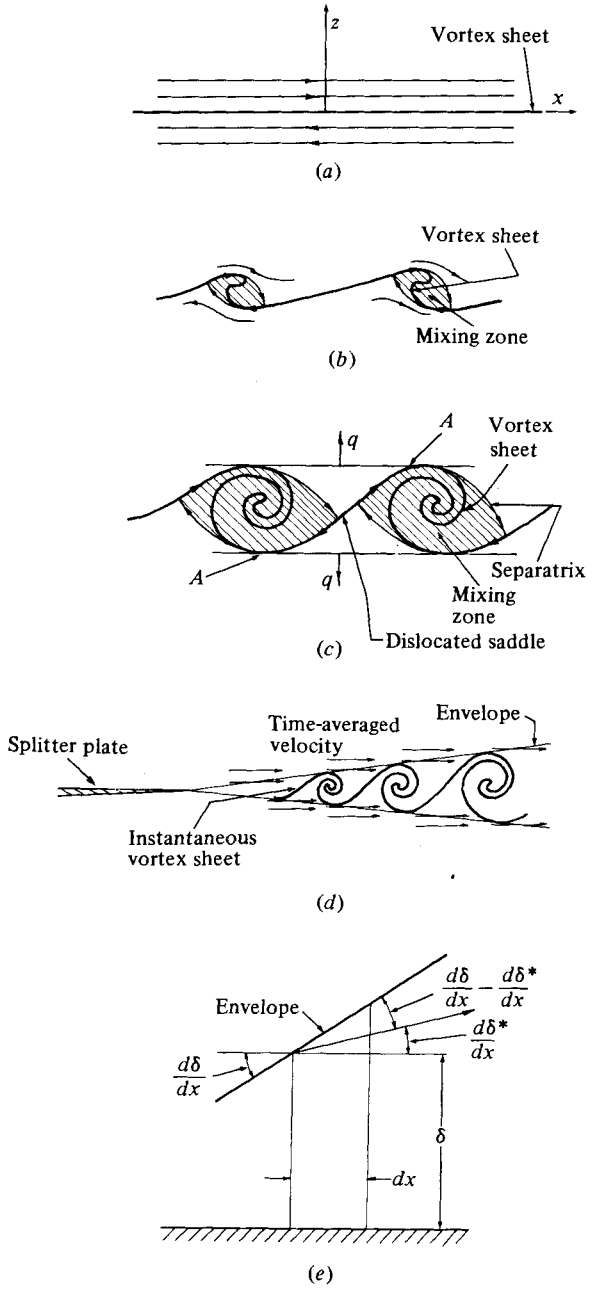

FIGURE 11. Progress of ideal Kelvin–Helmholtz-like roll-up of vortex sheet. (*a*) Undisturbed. (*b*) Initial roll-up. (*c*) Almost fully developed. (*d*) Developing shear layer behind a splitter plate. (*e*) Illustration of Head's definition of entrainment.

stretched into a spiral. Fluid bounded by the separatrices will ultimately acquire vorticity by viscous diffusion. As the structures grow, more fluid will be encompassed by the mixing zones. If vortex pairing occurs, the mixing zones would grow in a 'quantum jump' since all length scales would be doubled.

In three-dimensional flow mixing zones are more difficult to define since it might be possible for streamlines to enter regions of vortex sheet roll-up and leave without acquiring vorticity by viscous diffusion.

Returning to the two-dimensional Kelvin–Helmholtz-like roll-ups, the work of Winant & Browand (1974) and Brown & Roshko (1974) shows that these actually grow linearly with distance as shown in figure 11 (*d*). The time-averaged flow relative to an observer at rest with the origin of the shear layer is shown. The envelope which defines the region where mean flow has acquired mean vorticity is shown and fluid which is said to be entrained crosses this boundary. Figure 11 (*e*) shows how this definition is consistent with Head's (1960) definition. For boundary layers, the angle of the mean streamline at the envelope is $d\delta^*/dx$, where δ^* is the displacement thickness of the structure, whereas the outer boundary of the layer is at an angle $d\delta/dx$, where δ defines the outer envelope. Assuming that we are in a zero pressure gradient, the entrainment rate V is

$$V = U_1 \frac{d}{dx}(\delta - \delta^*), \tag{2}$$

which is the Head relation. It is assumed that the angles mentioned are small.

Returning to the structures described in § 3, a three-dimensional envelope could be constructed which would look like a fluted cone. Fluid crossing this envelope is said to be entrained. For the flow patterns shown in figure 9, fluid crossing this boundary will be referred to as entrainment of the second kind. This would include the fluid which moves towards the centres on the centre-plane or fluid which moves along alleyways and fluid which moves out in other planes. However, since this pattern is as seen by an observer moving with the structures, an additional volume of fluid is entrained because relative to this observer the envelope is propagating out as the structures grow with streamwise distance. This is entrainment of the first kind. The Head definition has been formulated for a stationary observer looking at boundary layers and wakes which are two-dimensional in the mean sense but the instantaneous flow patterns can be three-dimensional. For such flows if the observer and the structures are moving with a velocity U_ϕ, then entrainment of the first kind is $V_1 = U_\phi d\delta/dx$. This accounts for the outward movement of the envelope relative to the observer. Entrainment of the second kind due to flow spiralling in towards the centres or moving down alleyways will be written as V_2. Hence the total entrainment as seen by a moving observer is

$$V = U_\phi \frac{d\delta}{dx} + V_2. \tag{3}$$

This must be the same for a stationary observer and hence V given by equation (3) must be equal to that given by equation (2). This gives a relationship between V_2 and the standard mean flow quantities thus

$$V_2 = (U_1 - U_\phi)\frac{d\delta}{dx} - U_1 \frac{d\delta^*}{dx}. \tag{4}$$

These equations could be extended to three-dimensional mean flows if the shape of the envelope was known.

To summarize, there are basically two processes which govern entrainment. These are (*a*) the streamwise or time-wise growth of the envelope within which mean streamlines possess mean vorticity (entrainment of the first kind) and (*b*) the volume of fluid crossing this envelope by vortex induction and displacement thickness growth (entrainment of the second kind). The latter process can be seen quite clearly in figures 9(*a*) and (*b*).

5. Conclusions

The instantaneous flow fields surrounding the artificially stimulated coherent structures in nominally axisymmetric coflowing wakes of Perry & Lim have been measured. The vector fields were successfully obtained using a conditional sampling technique based on the precise phase of the disturbing oscillation. With the aid of critical point theory a qualitative description of the flow field has been obtained for all the simplest patterns classified by Perry & Lim, i.e. both coflowing jets and wakes. By relating these vector fields with the smoke patterns one can obtain an insight into how the smoke and vorticity from the source is convected and deformed. The process of entrainment of irrotational fluid is revealed very clearly from the vector field description.

This project was supported by the Australian Research Grants Committee and the Australian Institute of Nuclear Science and Engineering.

REFERENCES

ACHENBACH, E. 1974 *J. Fluid Mech.* **62**, 209.

BROWN, G. L. & ROSHKO, A. 1974 *J. Fluid Mech.* **64**, 775.

CANTWELL, B. J. 1975 A flying hot-wire study of the turbulent near wake of a circular cylinder at a Reynolds number of 140000. Ph.D. thesis. Cal. Inst. of Tech.

CANTWELL, B. J. 1978 *J. Fluid Mech.* **85**, 257.

CANTWELL, B. J., COLES, D. & DIMOTAKIS, P. 1978 *J. Fluid Mech.* **87**, 641.

CORCOS, G. M. & SHERMAN, F. S. 1976 *J. Fluid Mech.* **73**, 241.

DAVEY, A. 1961 *J. Fluid Mech.* **10**, 593.

DAVIES, P. O. A. L. & YULE, A. J. 1975 *J. Fluid Mech.* **69**, 513.

FALCO, R. E. 1977 *Phys. Fluids* vol. 20. No. 10 Pt. II, p. 124.

HEAD, M. R. 1960 *Aero. Res. Counc. R. & M.* 3152.

HEAD, M. R. & BRADSHAW, P. 1971 *J. Fluid Mech.* **46**, 385.

HUNT, J. C. R., ABELL, C. J., PETERKA, J. A. & WOO, H. 1978 *J. Fluid Mech.* **86**, 179.

LIGHTHILL, M. J. 1963 In *Laminar Boundary Layers* (ed. L. Rosenhead), pp. 48–88. Clarendon.

LIM, T. T. 1979 Coherent structures in coflowing jets and wakes. Ph.D. thesis, University of Melbourne.

OSWATITSCH, K. 1958 In *Die Ablonsungsbedingung von Grenzschichten. Grenzschicht Forschung* (ed. H. Goertler), p. 357. Springer.

PERRY, A. E. & FAIRLIE, B. D. 1974 *Adv. Geophys.* B **18**, 299.

PERRY, A. E. & FAIRLIE, B. D. 1975 *J. Fluid Mech.* **69**, 657.

PERRY, A. E. & LIM, T. T. 1978 *J. Fluid Mech.* **88**, 451.

PERRY, A. E. & WATMUFF, J. H. 1981 *J. Fluid Mech.* (to appear).

ROSHKO, A. 1954 *N.A.C.A. Rep.* no. 1191.

SMITH, J. H. B. 1972 *Prog. Aero. Sci.* **12**, 241.

TANEDA, S. 1978 *J. Fluid Mech.* **85**, 187.

WINANT, C. D. & BROWAND, F. K. 1974 *J. Fluid Mech.* **63**, 237.

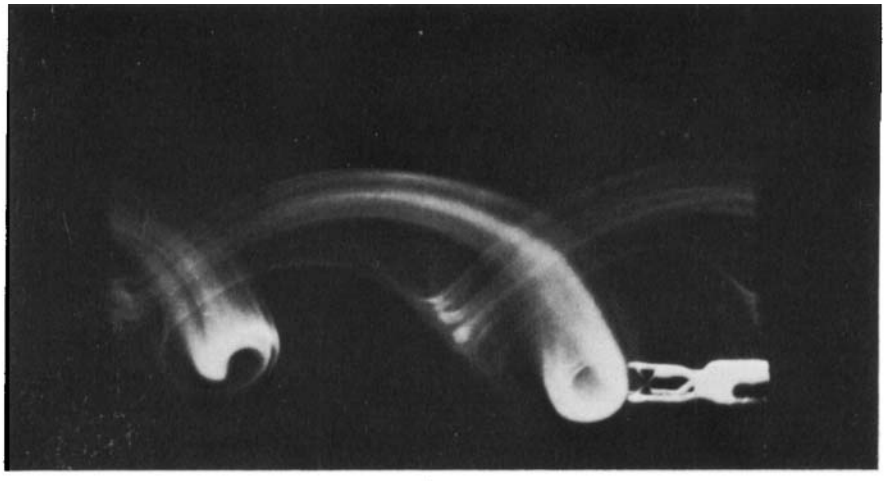

(*a*)

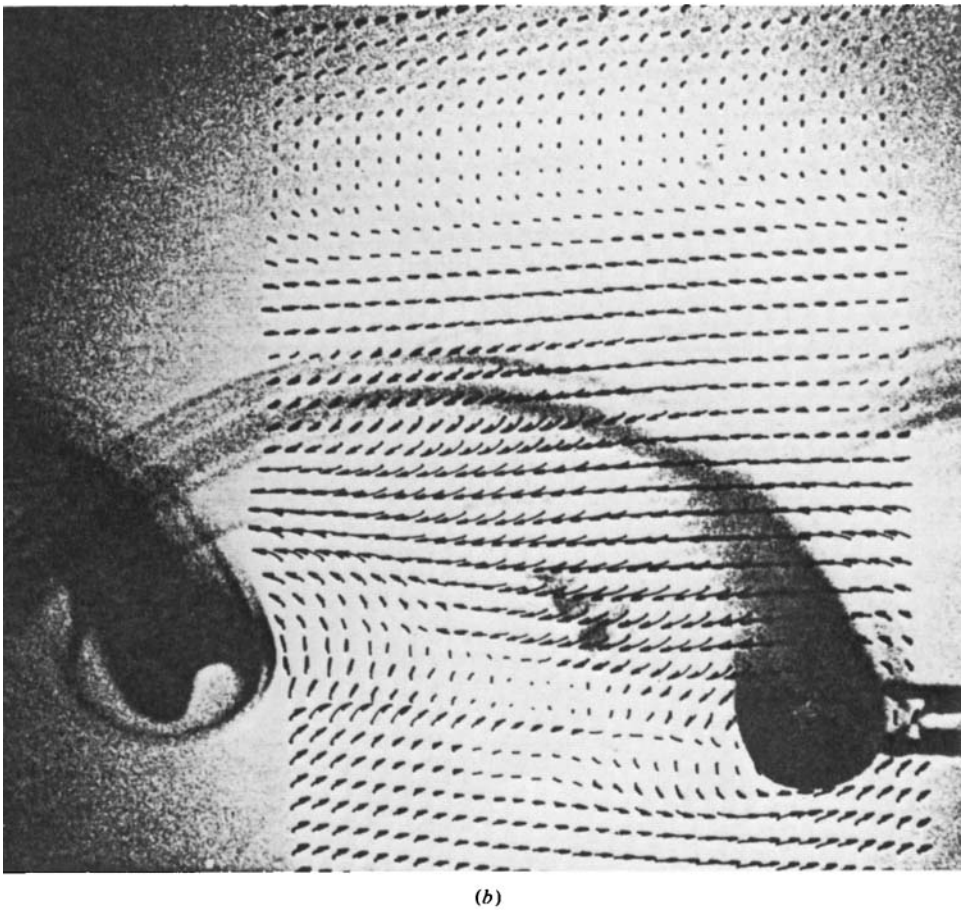

(*b*)

FIGURE 4. Simple negatively buoyant wake. (*a*) Smoke pattern; (*b*) superimposed photograph of smoke pattern and the velocity field. Reynolds number based on outer flow velocity and tube diameter (Re) = 400, frequency of vibration f = 8·5 Hz. Velocity of exit from tube very low.

(*a*)

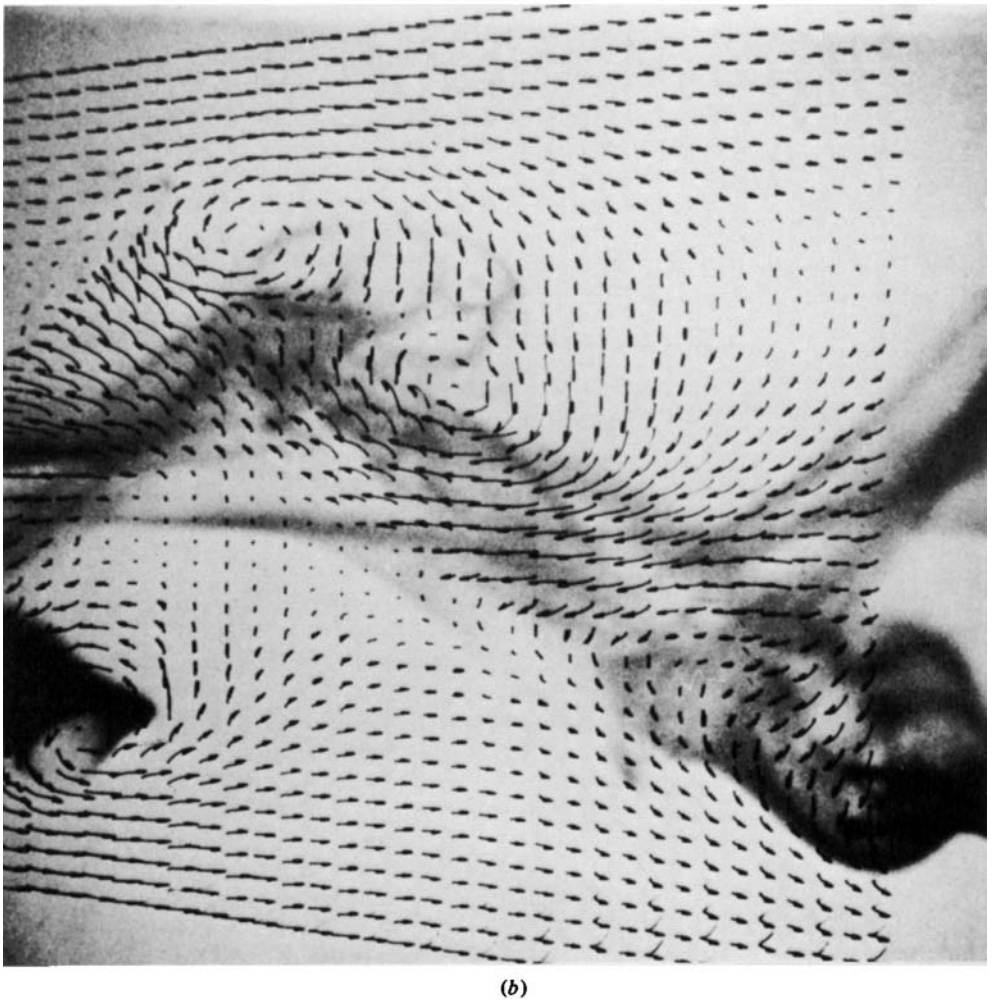

(*b*)

FIGURE 7. Neutrally buoyant wake. (*a*) Smoke pattern; (*b*) superimposed photograph of the smoke pattern and the velocity field. *Re* (based on outer flow) = 500, f = 10 Hz.

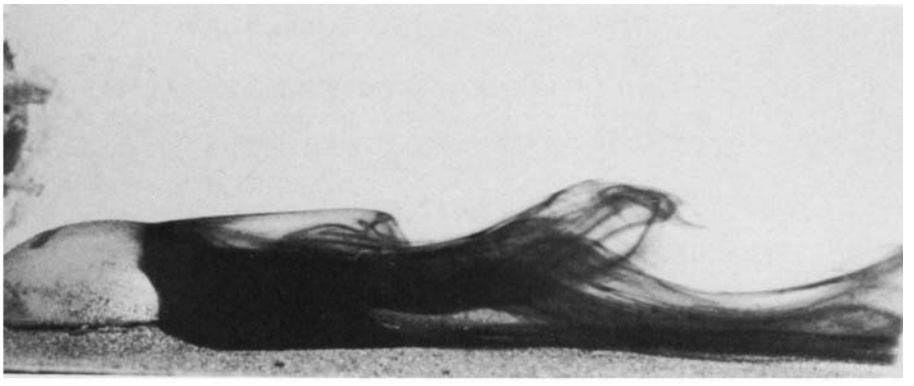

(*a*)

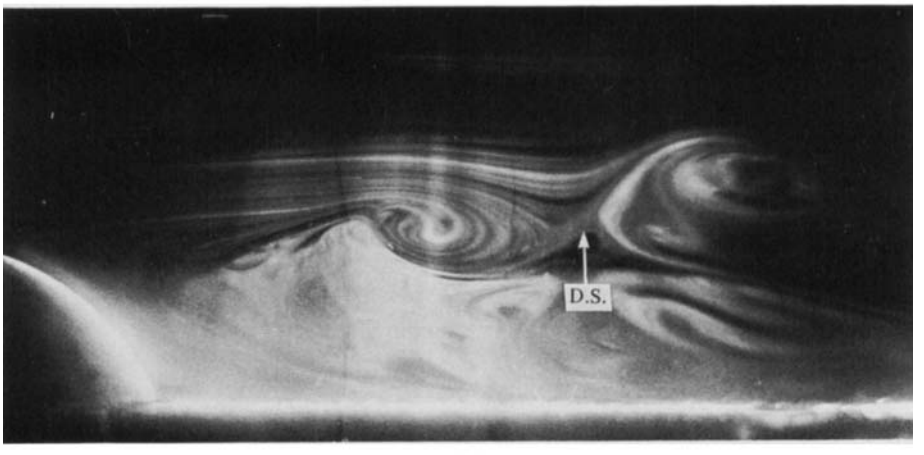

(*b*)

FIGURE 10. Flow over a rivet head. (*a*) Dye pattern. (*b*) Laser cross-section of dye introduced from upstream. Note the appearance of dislocated saddle. Reynolds number (based on the maximum height of the rivet) = 150. D.S. is a dislocated saddle.